Contents

Chapter 1

Introduction

Plasma medicine is an emerging field that is broadening its applications from uses on medical equipments (sterilization, decontamination) to uses on living tissues ([**IntoReview**]). One of the reserch groups working in RFX laboratories, in Padova, developed a source for the production of Cold Atmospheric Plasma (CAP) to be used for medical treatment on biological tissues ([1]). The source developed in this thesis is based on the DBD concept, where a dielectric is used to produce plasma with low charge density. It is developed to specializes in non thermal blood coagulation, i.e. acceleration of blood clot formation thanks to plasma direct application.

During this work we analyze prototypes alredy built, develop a new model and study how the source produces and expels plasma, with electrical measurements (chapter 2), high speed image acquisition (chapter **??**), plasma emission spectrum analysis (chapter **??**) and temperature measurements (chapter **??**).

1.1 Cold Atmospheric Plasma

Cold atmospheric plasma is a plasma at atmospheric pressure where there is not thermodynamical equilibrium between electron and ions, because electron temperature is much hotter then ion temperature ([**VONENGEL196599**]). In those conditions we can treat plasma as the collective motion of two interpenetrating fluids, where the thermal motion of ions can be ignored ([**goossens2012introduction**]). There are several studies on CAP plasma characteristics ([**Zhu_2009**], [**Ohyama_2009**], [**Amorim_2015**]) common values are electron temperatures $T_e = 1 - 10\,\mathrm{eV}$ and electron densities $n_e = 10^{17} - 10^{22}\,\mathrm{m}^{-3}$, inside the box outlined in figure 1.1.

1.1.1 Plasma generation: RF and DBD

Electron densities inside a cold plasma at atmospherci pressure are a small fraction of the neutral number density of an ideal gas $n_n = 2.50 \times 10^{25}\,\mathrm{m}^{-3}$, but higher then the number of electron-ion pair generated by radioactive substances and cosmic rays, ionization rate of $10^7\,\mathrm{m}^{-3}\mathrm{s}^{-1}$ ([**book:1593058**]). If we apply an electric field to a gas, electrons from

Figure 1.1: Plasma classification in function of electron density and electron temperature. Inside the square there are plasma with parameters typical for cold atmospheric plasma.

atoms or molecules are extracted thanks to the electric field separating electrons from ions or thanks to collisions with accelerated electrons, generating electron-ion pairs. Electrons acquire more energy from the applied electric field, due to the different mass and mobility, so electronic temperature increases more rapidly then ion temperature. If we use steady DC electric fields, electrons thermalize with ions trough collisions, generating thermal plasma at high temperatures. To produce cold plasma at high densities, we can give energy only to electrons with an electric field that changes in time, an AC field or a pulsed electric field ([**BARDOS20106705**]). Researchers at RFX developed sources functioning on RF and DBD principles (respectively [**Martines_2009**] and [1]).

RF source The RF source developed in RFX is composed by two coaxial tubes, the internal one is connected to a radio transmitter in series with a matching network and with an electrode formed by a wire grid, the external one ends with a second electrode fixed at ground potential, as in figure 1.2. The radio transmitter works with fixed power (5 W) and is set to a specific frequency that is the resonance frequency for the LC series circuit formed by the induttance in the matching network and the parasitic capacitance of the device. When neutral gas flows inside the inner tube, the electric field between the electrode ionizes it, producing cold plasma in air. The source is built with an induttance of 100 µH, capacitance is estimated as 10 pF, resulting in a resonance for a frequency around 4.8 MHz, reaching voltage peak to peak values of 900 V on the electrode. Regolation on the gas flow hallows to start the discharge more easily and to reach different peak voltage values. This source produces plasma directly in air, so it ionizes a mixture of neutral gas and air, giving birth to plasma rich in reactive species coming from oxygen and nitrogen molecules. The presence of reactive species hallow to use this source for non-

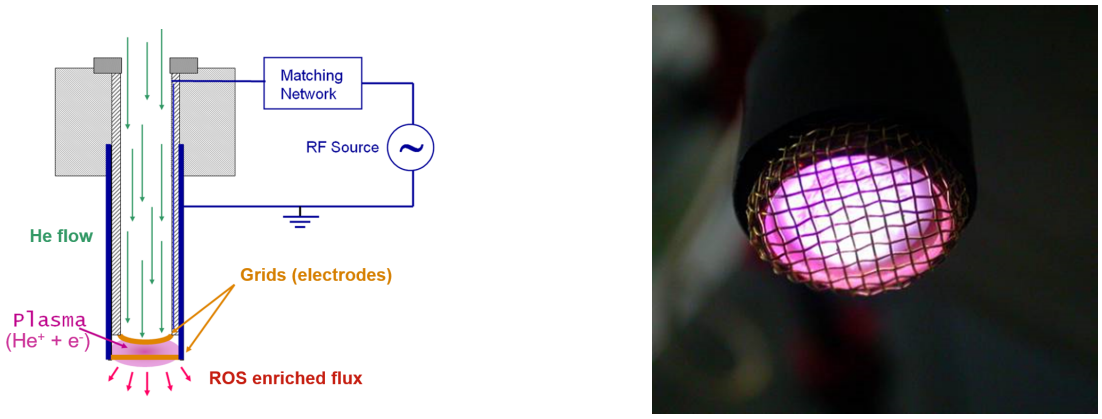

(a) Source scheme.

(b) Picture of produced plasma.

Figure 1.2: Plasma RF source developed in RFX.

thermal sterilization of living tissues, as is shown that this plasma has bactericidal effect without damaging human cells ([**doi:10.1002/ppap.200700154**], [**Stoffels_2007**]).

DBD source The principle used by the source developed with this work is that of Dielectri Barrier Discharge.

Image.

Dielectric shield.

Geometry, two electrodes.

1.1.2 CAP applications

CAPs are of particular interest in plasma medicine for two of their features:

- **Cold** : given non thermal equilibrium and ions low temperatures, those plasmas can be applied on surfaces without a dangerous increase in target temperature. In plasma medicine CAPs hallow plasma treatment on living tissues, where target temperature must stay below a certain temperature.
- **Reactive species** : if we produce plasma in atmospheric pressure, we can mix the gas used for plasma discharge with air. The peculiarity of a plasma in air is the presence of reactive species, ions, produced by ionization and recombination of nitrogen, oxygen, water and other atoms or molecules. In particular there are several biological processes where activation and reactions speed depend on concentration of Reactive Oxydant Species (ROS) and Reactive Nitrogen Species (RNS).

1.2 Plasma medicine

What we want, ROS, RNOS

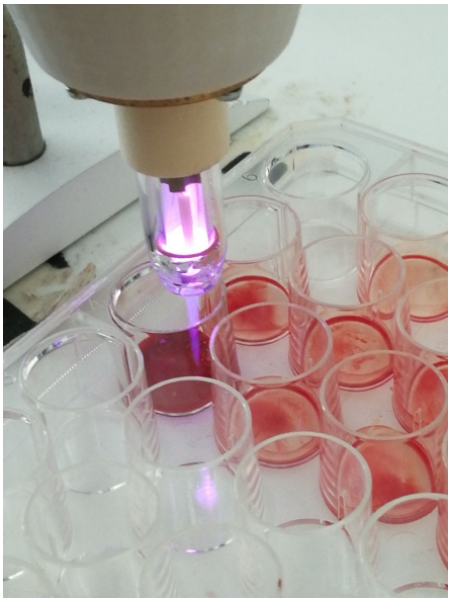

Figure 1.3: Picture of plasma application on blood samples.

- **Melanoma slowing**
- **Molecules delivery**

1.2.1 Bactericidal effects

disinfecting living tissues,

1.2.2 Blood coagulation

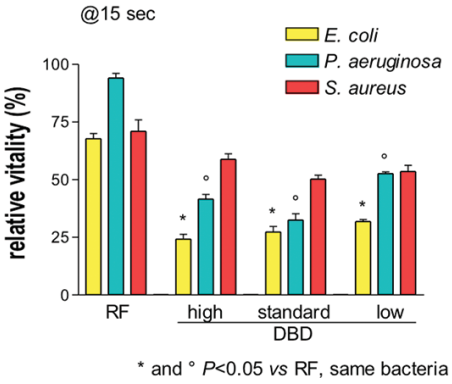

Figure 1.4: Relative vitality on different bacteria colonies after plasma treatment of 15 s with different sources and parameters. On the left treatment with an RF plasma source, on the right treatment with our DBD plasma source, for three different sets of discharge parameters (low, standard and high).

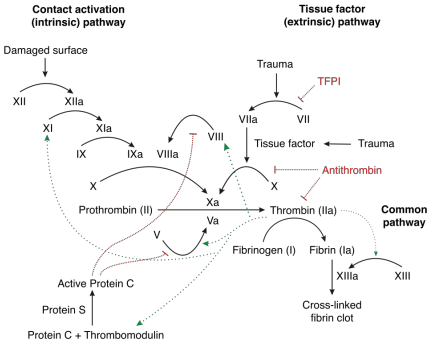

Figure 1.5: Schematization of processes leading to blood coagulation, we can see the two pathways, intrinsic and extrinsic, that ends in clot formation. The analysis of concentration of factors in blood samples treated with plasma, hallows to find where and how plasma intervenes in this scheme.

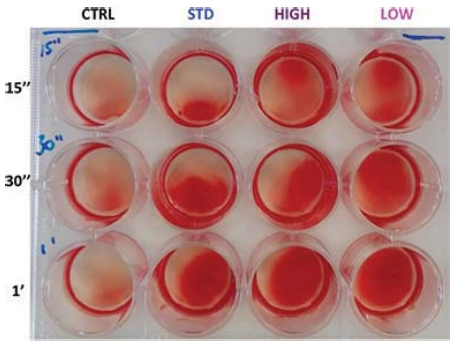

Figure 1.6: Blood samples after plasma treatment for different setups and application times. We can see absence of clot in control samples and clot formation where blood is treated.

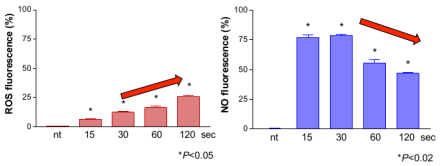

Figure 1.7: ROS and NO fluorescence

Chapter 2

Plasma source description and electric characterization

Plasma Coagulation Controller (PCC) developed at RFX is a DBD cold plasma source that produces plasma at atmospheric pressure. The entire design is developed to garantee the flexibility necessary to an easy use of the source. In this chapter we describe source functioning scheme and characterize it.

2.1 General source description

The source functions applying a fast high voltage pulse (from 2 to 10 kV) to a cyilindrical electrode covered by pyrex glass that works as the dielectric used to produce plasma in DBD conditions ([1]). The electrode is positioned along the axis of a nozzle where we insert neutral gas, a pure noble gas sometimes mixed with other gasses, that hallows to start the discharge. It is possible to put a second electrode formed by a conducting ring around the nozzle, that we can set to ground voltage or other voltage values, to modify the electric field if necessary.

When we send the voltage pulse, the electric field generated by the electrode ionizes the gas producing plasma with low free charge density thanks to the dielectric. Plasma forms a column of glowing gas, the plasma plume, that goes out from the nozzle exit and travels in the air outside, until it reaches a certain lenght or a target, as in figure 2.1. The plume is formed by cold plasma, it can be touched whitout a relevant increase of temperature on the skin or any other danger. In this work we want to study how the plume varies its traits changing futures in voltage pulse and used gas.

PCC development goes through different designs (an example of the first one in [**ceciliaDBD**]), for this study we use two different prototypes for the head, **A** and **B**, with same concepts and little differences.

In both models we have the high voltage controller separated from the head where plasma is produced, the first one controls the trigger for the voltage pulse, the second one is where we produce plasma. The two parts are connected only with power cables for the source and an optical fiber that sends the trigger for the voltage pulse. The

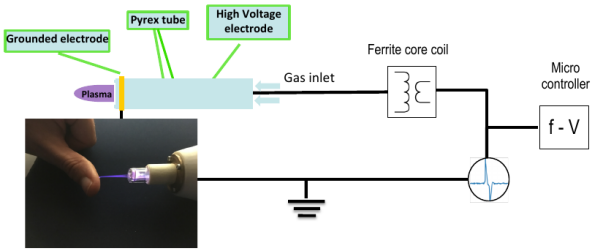

Figure 2.1: Scheme of source functioning. The micro-controller on the right sends a trigger signal to produce variable voltage on the coil mounted in the head, that produces an high voltage pulse on the electrode. The electric field ionizes the neutral gas and produces the plasma plume in the picture. The grounded ring around the nozzle is removable.

voltage pulse is created applying variable tension to a ferrite coil, where pulse repetition rate and voltage amplitude are controlled with an Arduino Leonardo mounted in the controller as explained later. The head is a cylinder 30 cm long with diameter of 8 cm, where are mounted three coils with three *N87* ferrite cores of dimensions $32 \times 16 \times 9$ mm and induttance 2.3 µH ([**N87datasheet**]). On every coil the spire ratio between primary and secondary circuit is of 1/30. The primary circuit is connected to the driver circuit that produces voltage variation, while the secondary circuit is connected to the electrode. Gas is inserted trough a separated channel that goes from one end of the source to the other end ends near the electrode. The nozzle at the end of the head can be selected between different materials and shapes. For this study we utilize a silicon nozzle that ends in a cylinder with a diameter of 1 mm and a cylindrical glass nozzle that shrinks at the end, until a diameter of 5 mm.

Prototype **A** is the first version used during this work, prototype **B** is the latest one, generally the second one is developed with higher ionization efficiency. Principal differences are:

- they have different geometries for the coils inside the head, so prototype **B** can produce higher voltage peak values;
- prototype **A** presents a problem of neutral gas diffusion in the area where there are the coils, in prototype **B** the two areas are not in communication (except for the electric connection of the electrode).

2.2 Electric scheme

In this chapter is discussed the development of Plasma Coagulation Controller eletcric scheme and its characterization. Circuit design, as the entire model design, is highly influenced by needs of flexibility and mobility of the source for wound treatment. To produce plasma as DBD, in air, with helium or argon as ignition gasses, it is necessary to

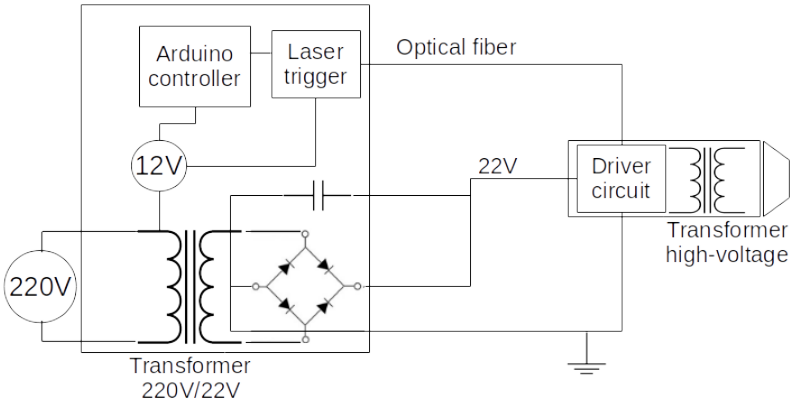

Figure 2.2: Scheme of the general electric line to produce high voltage, the controller on the left and the head on the right.

apply high electric fields in little space. Manwhile, to make possible easy medical application the source head (where there si plasma output) must be compact, with particular attention to electric safety measuraments. It is common to produce electric fields with fast voltage pulses for various uses, including jet or DBD plasma production ([2], [3], [4])), the scheme used in this study outputs a voltage pulse with an amplitude from 1 kV to 10 kV and pulses frequencies from 5 kHz to 60 kHz.

A rappresentation of power and signal lines is in figure 2.2. The circuit is divided mainly in two parts : the controller, with alimentation and settings controls, and the head, where the discharge happens and plasma is emitted.

Lines divides in:

- **Alimentation** : the 220 V DC power line goes in a transformer that gives a reduced tension to the head, 22 V in the figure, passing through a diode bridge. This tension aliments the Driver Circuit on the head.

- **Arduino and trigger** : the power line is reduced to 12 V necessaries to aliment an Arduino controller and a laser. From an Arduino analogical output a PWM wave goes to the laser trigger, it transmits information on the wave, frequency and duration, with an optical fiber that ends with a photodiode installed on the driver circuit. Wave frequency is setted by the Arduino, wave duration is setted giving the opening time of the MOSFET that passes the signal to be amplified and sent to the head's transformer. With this setup the high-voltage line is entirely decopuled from the controller, so there are not problems of signal reflection on the power line

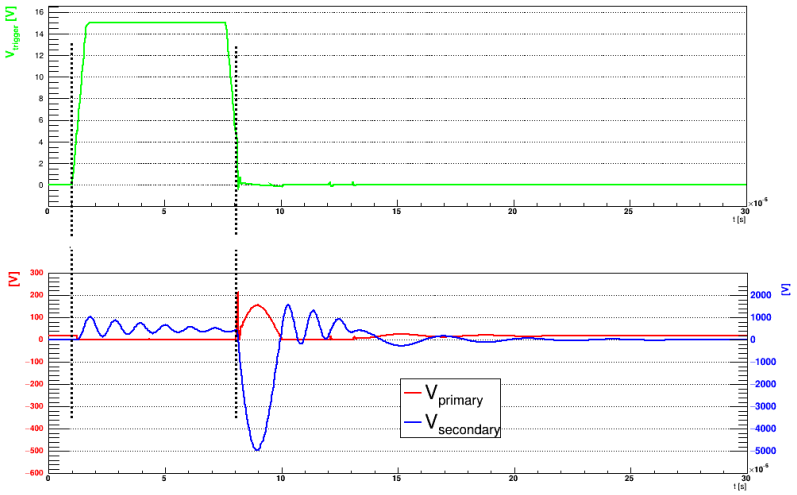

Figure 2.3: Scheme of signal propagation. Up, in green, there is the optical trigger, down, in red, the voltage of primary circuit in the head with axis on the left, in blue, the voltage of secondary circuit with axis on right.

or the Arduino.

- **Head** : the Driver Circuit receives a power line and an optical trigger that defines frequency and duration of the voltage pulse. When the trigger gives the start signal, the transformer on the head receives on primary circuit a voltage of hundreds V and outputs from secondary circuit a voltage of thousends V. Connected to the output there is the electrode inside a capillary tube of dielectric material.

To understand signal propagation is presented a simulation in figure 2.3, obtained with a simplified scheme with Spice. As shown, once the PWM trigger starts, tension on the primary goes from alimentation value to 0, when the PWM signal ends (after 6 µs, it has a pulse with amplitude of 150 V (width of 1.2 µs) and a pulse of −5000 V at the output of secondary circuit. A longer PWM implies a longer charging time, so an higher pulse. Ultimately, amplitude of the pulse is proportional to the width of the PWM signal and to know working conditions of the source it is necessary to study relation between opening time and amplitude output on the actual circuit.

During this thesis study were built two sources, with two controllers and heads, the first one will be called source A, the second one source B. From an electrical perspective the two models are almost identical, the second one comes with a low-pass filter on the driver circuit (to diminish high frequencies noise) and higher amplitude capabilities thanks to a different turns ratio in head's transformer. The characterization of electric features is made measuring output tension and current with different settings.

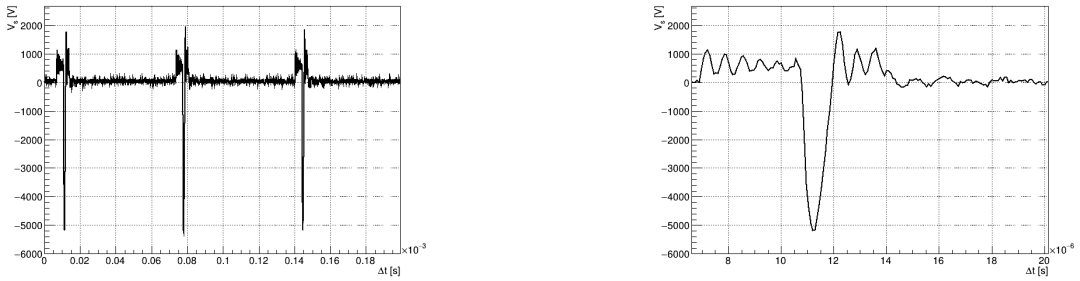

(a) Three pulses

(b) Zoom on one pulse

Figure 2.4: Example pulses with source B for $f = 10\,\text{kHz}$ and $\Delta t = 2\,\mu\text{s}$

2.3 Output characterization

Plasma ignition and discharge features are regolated by electric field generated in the circuit head and power deposition to flowing gas, so the parameters involved are pulse amplitude and frequency arriving on the electrode, settable in the circuit. Medical application of plasma requires low current intensity, in this study it's measured current intensity flowing on a copper sheet targeted by the plasma plume at a certain distance. Ultimately the different parameters for the measures are: Δt, opening time of the trigger that defines amplitude of the pulses, and f, frequency of the pulses.

Voltage signals are taken with an high-voltage probe *Tektronix P6015A*, attenuation $\times 1000$, current signal with a *Tektronix CT2* probe that gives a 1 mV for a current of 1 mA. All signals are measured with a *Yokogawa DL9040* oscilloscope, from which is saved the waveform of voltage and current.

Measures are taken without gas flowing, to see clean output voltage of the circuit, and with an helium flow of 2 L/min, to measure the actual output in presence of plasma, with different amplitude and frequencies. It's also measured an effective current intensity, i.e. a mean value in a time period, to evaluate plasma application's effects on biological tissues.

Every lenght measure is done with a decimal caliper, it's taken an uncertainity of 0.1 mm.

2.3.1 Measures without gas

It's used the hv probe to pick tension's differences between secondary circuit ouput and ground. Once a work frequency, f, is set, we take voltage wave shape for different values of opening time of the circuit, Δt, in the selectable range. To assure that a voltage pulse ends before another starts, this range is different for different frequencies: higher work frequencies means more pulses in a given time, taking into consideration pulse oscillations, the range of possible Δt is smaller at higher frequencies. A typical measure is shown in figure 2.4.

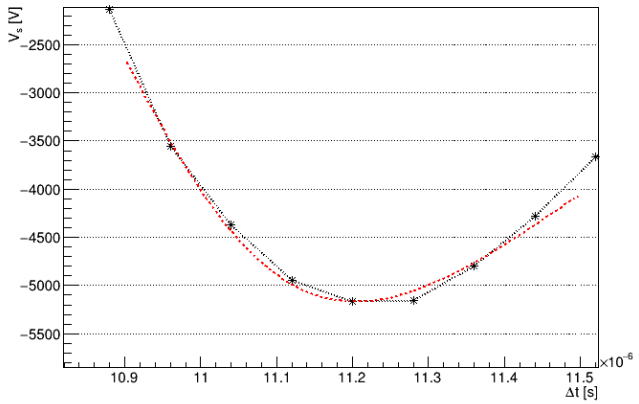

Figure 2.5: Example fit with source B for $f = 10\,\text{kHz}$ and $\Delta t = 2\,\mu\text{s}$

The main pourpous of the measures is to study proportionality between amplitude of the peak and opening time, for different frequencies. Those signals are analyzed evaluating their Fourier Transform (using ROOT C++ libraries [5]) and reconstructing the signal without higher frequencies, to exclude noise fluctuations. The reconstructed peak is an asymmetric function in time as in figure 2.5, it's possible to interpolate it with a Landau function [6] and obtain peak value and position. The error from the fit function is added quadratically to the error given by the cut of high Fourier frequencies, evaluated as the square root of the mean square difference between reconstructed and original signal for every point included in fit range.

Results are shown in figure 2.6 for the two sources. In source A we can see a linear behavior for $4 \leq \Delta t \leq 16\,\mu\text{s}$, with tensions from 2.02 ± 0.01 to $9.25 \pm 0.05\,\text{kV}$; for greater Δt data loses linearity. The upper limit on chosen Δt is given by the need of a minimum time interval between two pulses. Also in source B we can see a linear behavior, but tension values are larger, for $1 \leq \Delta t \leq 8\,\mu\text{s}$ tension goes from 3.66 ± 0.06 to $11.76 \pm 0.22\,\text{kV}$. With this source the upper limit for Δt is chosen observing voltage output: measures are taken only for tensions needed to have plasma in a DBD regimen, higher opening times would only stress more circuit components. Both sources have near the same output for different frequencies, to confirm it datas are fitted with a linear function in the range $0-16\,\mu\text{s}$ for source A and range $0-8\,\mu\text{s}$ for source B. Evalueted parameters are compared, as shown in figure 2.7. The values are displaced with random distances from the mean value, so it can be concluded that the behavior is not defined by the frequency.

2.3.2 Measures with gas

Introduction of an helium flow at the end of the head will produce plasma ignition, tension will be different, and it will be possible to measure current intensity carried by plasma. To assure safety of plasma application, that cells aren't damaged by plasma, it must be avoided a large current intensity and arc formation. Studies of conditions for

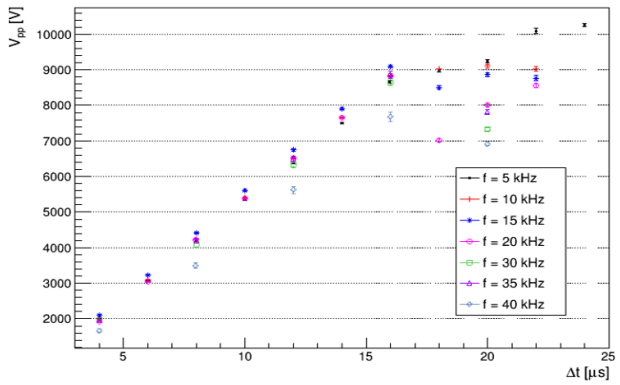

(a) Source A

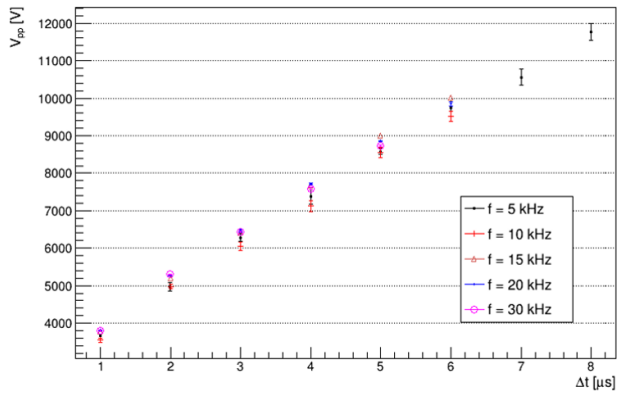

(b) Source B

Figure 2.6: Absolute peak's value of secondary circuit in function of Δt at different f, for both sources.

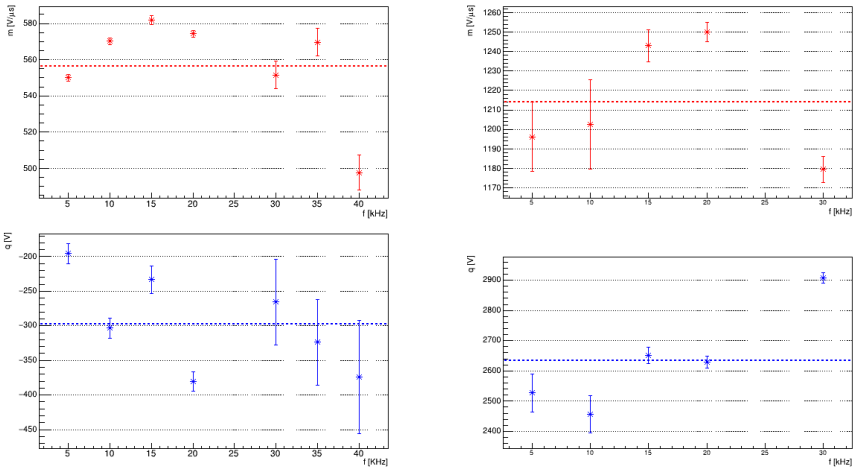

(a) Source A **(b)** Source B

Figure 2.7: Voltage peaks are fitted with a linear function $V_{peak} = m\Delta t + q$, in figure we see fit parameters at different frequencies for both sources, in dashes the mean value.

DBD discharges and arc transitions ([7], [8], [9]) suggests that for fast pulses it's safe to have current intensity $< 10\,\text{mA}$.

Current intensity is measured using a copper sheet with dimensions $10\,\text{mm} \times 10\,\text{mm} \times 1\,\text{mm}$. Plasma plume impacts on the sheet, the current probe is connected to it and sends a voltage signal to the oscilloscope, with cable shielding to lessen interferences. Current intensity and target distance relation is studied in[10], in this study the distance between target and electrode is chosen around typical value for treatments permitted by head's sources geometry: $10\,\text{mm}$ for source A and $15\,\text{mm}$ for source B (a bit longer due to electrode position in the head).

In figure 2.8 can be seen a typical measure for $\Delta t = 8\,\mu\text{s}$ and $f = 5\,\text{kHz}$ with source B. For both sources there is a current peak in correspondence of voltage pulse that increases with tension, however for source B there are measures where the peak is so low that it is covered by noise.

Data analysis is done as before, cleaning measures from noise, estimating the peak and it's error. Results are shown in figures 2.9 and 2.10, measures where the current peak is not distinguishable are excluded from plots.

Tension peaks are slightly lower then values without gas, as expected seeing the plume as an additional load at the end of the circuit ([11]), but the linear behavior for $V_{pp} \leq 10\,\text{kV}$ remains and we can compare linearity for different frequencies. Current intensities grows with tension and are higher for source A, as expected given different distances electrode-target. Analysis of linearity also for those measures can show if there is a different behavior changing pulse frequency or source. Figures 2.11 and 2.12 shows results of the linearity study at different frequencies. Tension values, for both sources, are scattered around the mean value parameter without a clear behavior, confirming

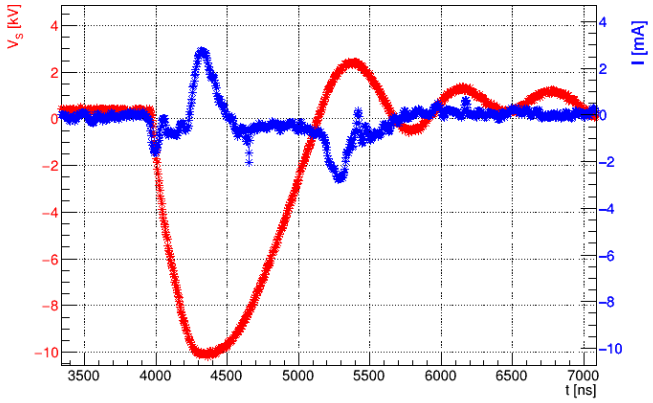

Figure 2.8: Example measure with source B for $f = 5\,\text{kHz}$ and $\Delta t = 8\,\mu\text{s}$

independence hypotesis of voltage growth from pulses frequencies. For source A we find a slope parameter $m_V = 0.366 \pm 0.001\,\text{kV}/\mu\text{s}$, for source B $m_V = 1.145 \pm 0.008\,\text{kV}/\mu\text{s}$, larger due to the different circuit, as mentioned before. Current values shows a different behavior: in source A we find a stady increase of parameters with higher frequencies, in source B data are more scattered and we couldn't extrapolate a behavior. However current slope is in the same range of values for the sources, with a maximum for source A of $m_I = 1.10 \pm 0.01\,\text{mA}/\mu\text{s}$ and for source B of $m_I = 1.04 \pm 0.17\,\text{mA}/\mu\text{s}$. An explanation for parameter's trend in source A it's that for higher frequencies the interval between two pulses it's smaller and oscillations of electrode potential after a pulse influences more gas ionized fraction, so mean density value of charged particles is higher for higher frequencies. Due to low signal to noise ratio in measures for source B, it is not possible to esclude a relation between current slope (how much current intensity grows increasing opening time) and pulse frequency, however it is established a maximum limit value to take into consideration when using the device.

2.3.3 Plasma impedance

From tension and current measuraments we can define plasma's electric behavior, in this subsection source B measures are used to estimate plasma impedance. Tension output from head's transformer can be modelized as a dumped sine wave around the peak, as in equation 2.1.

$$V_S = V_0 + V_{\text{pulse}} \sin\left(2\pi f_{V_s} t\right) e^{-t/\tau} \tag{2.1}$$

This formula gives an explicit parametrization for f_{V_s} that is an estimation of the frequency of the single pulse (the frequency that defines rise and fall of the pulse, different from the work frequency of different pulses imposed by Arduino, called f). This parameter is important because plasma's electric behavior depends on this frequency, analyzing

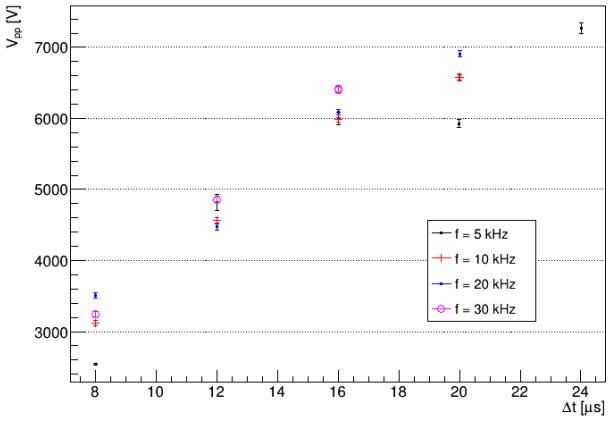

(a) Source A

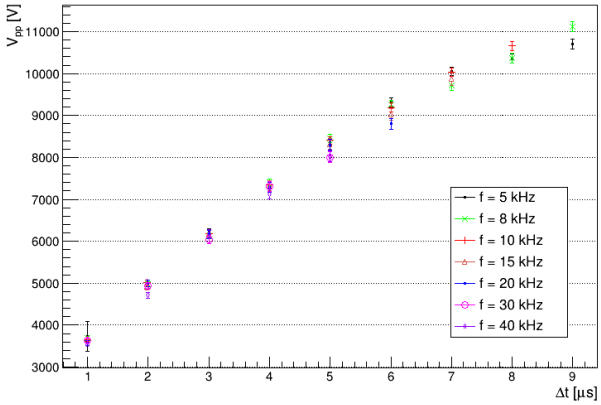

(b) Source B

Figure 2.9: Absolute peak's values of secondary circuit output in function of Δt at different f, with an helium flux of 2 L/min, for both sources.

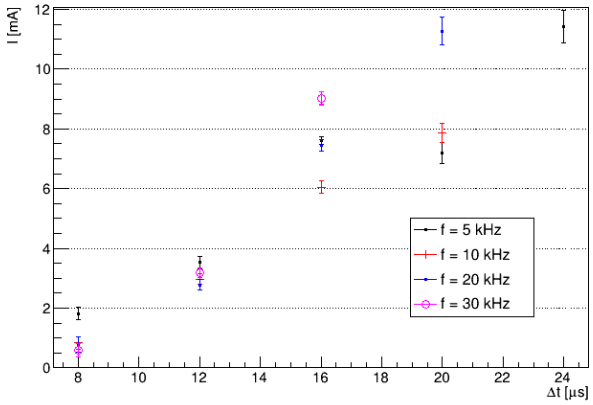

(a) Source A

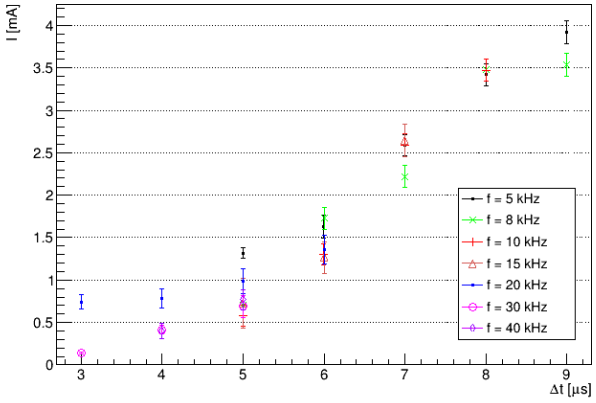

(b) Source B

Figure 2.10: Absolute peak's value of current intensity on copper target with an helium flux of 2 L/min, in function of Δt at different f, for both sources.

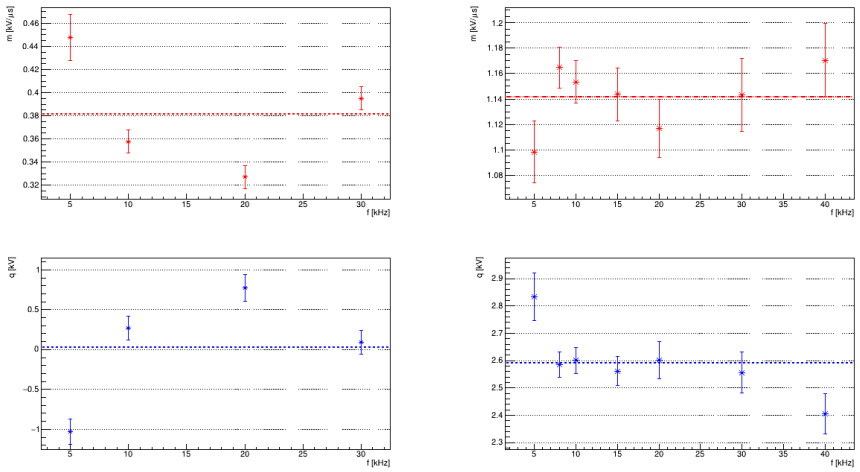

(a) Source A **(b)** Source B

Figure 2.11: Voltage peaks are fitted with a linear function $V_{peak} = m\Delta t + q$, in figure we see fit parameters at different frequencies for both sources, in dashes the mean value.

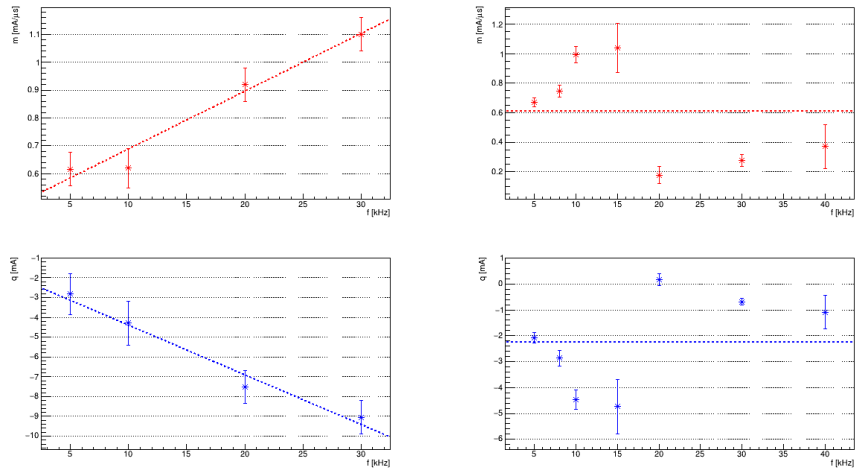

(a) Source A **(b)** Source B

Figure 2.12: Current peaks are fitted with a linear function $I_{peak} = m\Delta t + q$, in figure we see fit parameters at different frequencies for both sources. For source A we see in dashes a linear fit, for source B the mean value.

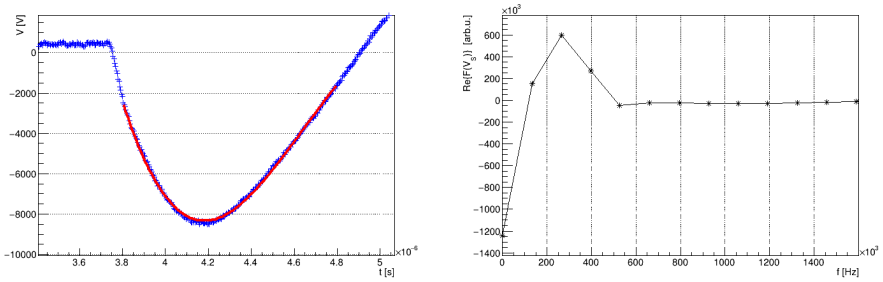

(a) Dumped sin fit **(b)** Fourier transform

Figure 2.13: On the left example fit of a tension peak, $f = 8\,\text{kHz}$ $\Delta t = 5\,\mu\text{s}$ with function 2.1; on the right the fourier transform of the measure in the interval $[3 - 6\,\mu\text{s}]$ that shows the frequency peak f_{V_s}

signal with different frequencies f_{V_s} it's possible to understand plasma's parameters. Frequency pulse it's different for every opening time of the circuit, Δt, but it's constant when changing frequency of pulses, as explained before analyzing tension outputs at different frequencies. In figure 2.13 are presented examples of a peak fitted with the function in formula 2.1 and it's fourier transform to show peak frequency corresponding to f_{V_s} for that specific Δt. In figure 2.14 are shown different resulting parameters for different Δt.

Fit parameters follows always those presented: as expected, with higher opening times V_{pulse} grows while f_{V_s} and τ have their own behaviors that depends from tension secondary output V_s. To estimate plasma's impedance it's useful to observe that voltage peak is quite large in time: it varies of less then 3% of peak's value in an interval of 150 ns around it. As tension and current peaks times differs always by a time interval $|t_{V_p} - t_{I_p}| \leq 150\,\text{ns}$, it's possible to assume $V_{t_{I_p}} \simeq V(t_{V_p})$, i.e. that tension during the current peak maximum is equal to tension's peak value. With this approximation, it makes sense to plot tension's peak values against current's peak values, as in figure 2.15, and given a Δt it's possible to give an estimation of impedance module as $Z = \frac{V_p}{I_p}$. Resulting impedance are shown in figure 2.16, changing opening times and changing frequency of single pulse f_{V_s}.

From the graphs it's possible to extrapolate that plasma impedance goes from $2.98 \pm 0.11\,\text{M}\Omega$ to $11.82 \pm 2.19\,\text{M}\Omega$, with near constant values in the range of opening times $7-9\,\mu\text{s}$. From a deeper analysis and specific measures it could be possible to expand the analysis here presented and estimate plasma's electrical resistance, capacitance or induttance.

2.3.4 Effective current

Current effects in applications on biological tissues have to take into consideration current intensity in a time interval tipically larger then the pulse widths used in our sources ([12], [10]). It's possible to estimate an effective current that is more appropriate to take into consideration when evaluating damage due to currents, as a mean of current intensity in a defined time interval calculated with equation 2.2, taking $t_2 - t_1 = 1\,\text{ms}$. The effective

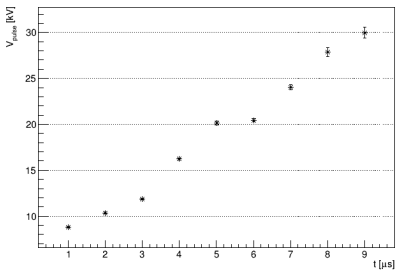

(a) V_{pulse}

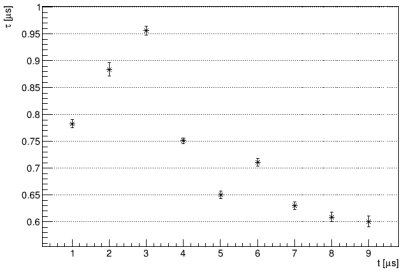

(b) τ

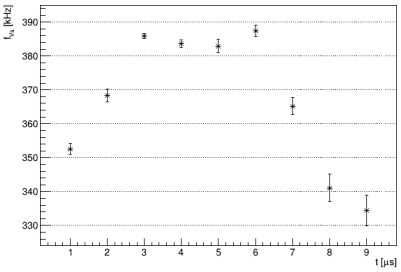

(c) f_{V_s}

Figure 2.14: Fit parameters of pulses with $f = 8\,\text{kHz}$ for different Δt.

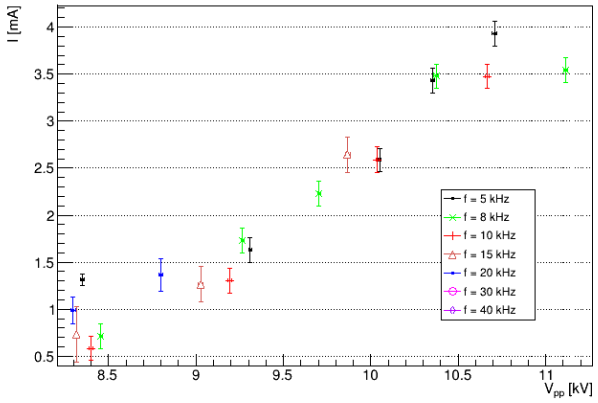

Figure 2.15: Tension's peak values against current's peak values for different Δt and frequencies.

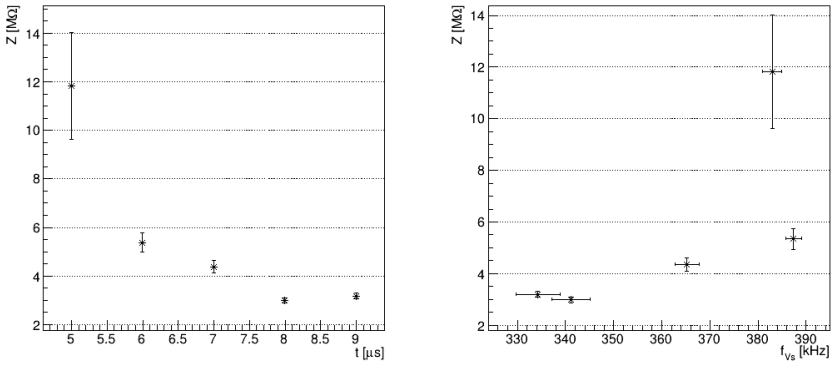

Figure 2.16: Impedance module estimation for different opening times (left) corresponding to different frequencies (right).

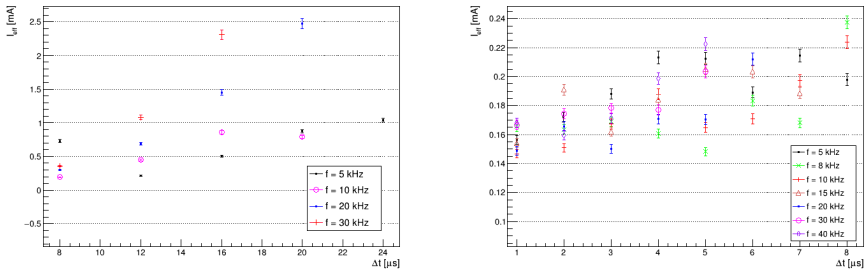

(a) Source A **(b)** Source B

Figure 2.17: Effective currents in a time interval of 1 ms.

current takes into consideration that current values are very small for all the time between two pulses.

$$I_{\text{eff}} = \frac{1}{(t_2 - t_1)} \sqrt{\int_{t_1}^{t_2} I^2 \, dt} \tag{2.2}$$

Figure 2.17 shows effective currents measured for both sources. Values are significantly smaller then maximum peak values, expecially for source B where oscillations after the main peak are smaller. The maximum value for the two sources is given by $I_{\text{eff}A} = 2.47 \pm 0.07\,\text{mA}$ and $I_{\text{eff}B} = 0.23 \pm 0.01\,\text{mA}$.

2.3.5 Time intervals

Time width of signal affects reaction's probabilities (chapter **??**) and plasma's power deposition(chapter **??**), here we try to give an estimate of those time intervals. It can be defined as the FWHM of measured peaks, evaluated as the time when we measure half

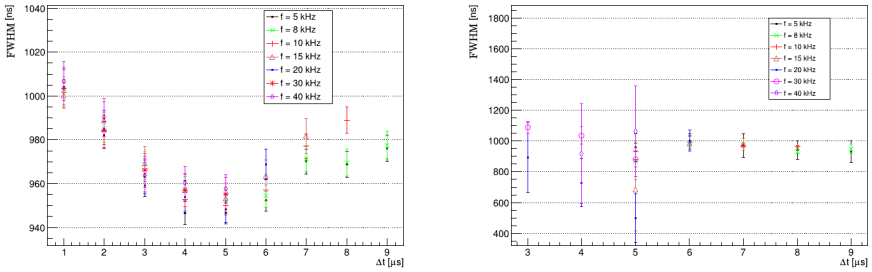

(a) Voltage **(b)** Current

Figure 2.18: FWHM of tension and current peaks varying opening time, for different frequencies.

of tension or current maximum value. As the characterization of the sources shows an almost equal behavior, this study is made only for the latest version of the source, that's the only one used in the following chapters. Results are shown in figure 2.18. For every frequence there is a quadratic behavior of tension widths with a minimum for a $\Delta t = 5\,\mu s$ that depends on circuit scheme. It is possible to give an estimation of pulse width with a mean value between this minimum and maximum values obtained for $\Delta t = 1\,\mu s$, it is $T_V = 963 \pm 15\,ns$. For currents, widths have great uncertainity where the peak is low, but it is possible to evaluate a mean value for $\Delta t \geq 6\,\mu s$, and it is $T_I = 968 \pm 28\,ns$. Values from the two measures are compatible and they are a good estimation of pulse time duration.

Bibliography

[1] Gianluca De Masi et al. "Plasma Coagulation Controller: A Low- Power Atmospheric Plasma Source for Accelerated Blood Coagulation". In: *Plasma Medicine* 8.3 (2018), pp. 245–254. ISSN: 1947-5764.

[2] J. Upadhyay et al. "Development of high-voltage pulse generator with variable amplitude and duration". In: *Review of Scientific Instruments* 85.6 (2014), p. 064704. DOI: 10.1063/1.4884883.

[3] Julien Jarrige, Mounir Laroussi, and Erdinc Karakas. "Formation and dynamics of plasma bullets in a non-thermal plasma jet: influence of the high-voltage parameters on the plume characteristics". In: *Plasma Sources Science and Technology* 19.6 (2010), p. 065005. DOI: 10.1088/0963-0252/19/6/065005. URL: https://doi.org/10.1088%2F0963-0252%2F19%2F6%2F065005.

[4] T Darny et al. "Analysis of conductive target influence in plasma jet experiments through helium metastable and electric field measurements". In: *Plasma Sources Science and Technology* 26.4 (2017), p. 045008. DOI: 10.1088/1361-6595/aa5b15. URL: https://doi.org/10.1088%2F1361-6595%2Faa5b15.

[5] *ROOT documentation for TVirtualFFT class*. URL: https://root.cern.ch/doc/master/classTVirtualFFT.html.

[6] R. Brun. *ROOT documentation for Landau() function*. 1995. URL: https://root.cern.ch/doc/master/namespaceTMath.html#a656690875991a17d35e8a514f37f35d9.

[7] U. Kogelschatz, B. Eliasson, and W. Egli. "Dielectric-Barrier Discharges. Principle and Applications". In: *Journal de Physique IV Colloque* 07.C4 (1997), pp. C4–47–C4–66. DOI: 10.1051/jp4:1997405. URL: https://hal.archives-ouvertes.fr/jpa-00255561.

[8] Takaaki Tomai, Tsuyohito Ito, and Kazuo Terashima. "Generation of dielectric barrier discharge in high-pressure N2 and CO2 environments up to supercritical conditions". In: *Thin Solid Films* 506-507 (2006). The Joint Meeting of 7th APCPST (Asia Pacific Conference on Plasma Science and Technology) and 17th SPSM (Symposium on Plasma Science for Materials), pp. 409 –413. ISSN: 0040-6090. DOI: https://doi.org/10.1016/j.tsf.2005.08.101. URL: http://www.sciencedirect.com/science/article/pii/S0040609005013052.

[9] Lewi Tonks and Irving Langmuir. "A General Theory of the Plasma of an Arc". In: *Phys. Rev.* 34 (6 1929), pp. 876–922. DOI: 10.1103/PhysRev.34.876. URL: https://link.aps.org/doi/10.1103/PhysRev.34.876.

[10] Cecilia Piferi. "Caratterizzazione di sorgenti di plasma per applicazioni biomediche". 2016/17.

[11] M.A. Lieberman and A.J. Lichtenberg. *Principles of Plasma Discharges and Materials Processing*. Wiley, 1994. ISBN: 9780471005773. URL: https://books.google.it/books?id=-cloQgAACAAJ.

[12] Stephanie Tümmel et al. "Low Temperature Plasma Treatment of Living Human Cells". In: *Plasma Processes and Polymers* 4.S1 (2007), S465–S469. DOI: 10.1002/ppap.200731208. eprint: https://onlinelibrary.wiley.com/doi/pdf/10.1002/ppap.200731208. URL: https://onlinelibrary.wiley.com/doi/abs/10.1002/ppap.200731208.